







Coconut Husk Fiber: A Low-Cost Bioresource for the Synthesis of High-Value Nanocellulose

Chidamparam Poornachandhra¹ , Rajamani M. Jayabalakrishnan^{1,*} 
Govindaraj Balasubramanian² , Arunachalam Lakshmanan³ , S. Selvakumar⁴, Muthunalliappan Maheswari⁵ , Joseph Ezra John⁵ 

¹ Department of Environmental Sciences, Tamil Nadu Agricultural University, Coimbatore, India; poorna155c@gmail.com (C.P.); jayabalphd@gmail.com (R.M.J.);

² Agricultural College and Research Institute, TNAU, Karur, India; agribalu@live.in (G.B.);

³ Department of Nano Science and Technology, Tamil Nadu Agricultural University, Coimbatore, India; microlaxman@gmail.com (A.L.);

⁴ Agricultural Engineering College and Research Institute, TNAU, Coimbatore, India; engineerselva@yahoo.co.in (S.S.);

⁵ Department of Environmental Sciences, Tamil Nadu Agricultural University, Coimbatore, India; maheswarisekar2004@yahoo.com (M.M.); ezrajohn4@gmail.com (J.E.J.);

* Correspondence: jayabalphd@gmail.com (R.M.J.);

Scopus Author ID 16230026200

Received: 17.10.2022; Accepted: 24.11.2022; Published: 31.01.2023

Abstract: Nanocellulose has recently gained a foothold of significance among nanomaterials due to its unique properties, including renewability and sustainability. In this study, two promising methods, steam explosion and alkali-acid hydrolysis, were evaluated for the cellulose extraction from coconut husk fiber. Between the two methods, alkali-acid hydrolysis yielded 1.8 times higher cellulose content than the other. Hence, cellulose was obtained through the alkali-acid hydrolysis method to synthesize Nano-Crystalline Cellulose (NCC). In order to maximize cellulose content in nanocellulose synthesis, acid concentration, reaction temperature, and hydrolysis time were optimized using Response Surface Methodology (RSM). The optimum reaction condition for the synthesis of NCC was 50 °C with 45 wt% acid concentration for 60 minutes due to its high cellulose content (85.6 %). Synthesized NCC was spherical in shape with a diameter below 40 nm. NCC had better crystallinity (80.05 %) with a high zeta potential of -72.2 mV. NCC was evaluated for its adsorption capacity for different dyes at varying pH levels. Among the dyes, the removal efficiency of NCC was higher for methylene blue (90.89 %) and congo red (89.96 %) at all pH levels. But adsorption of crystal violet dye by NCC was higher in alkaline pH (9) and methyl red in acidic pH (5). As a result, synthesized nano cellulose could be used in the removal of synthetic dyes from textile effluents.

Keywords: coir fiber; steam explosion; alkali-acid hydrolysis; nanocrystalline cellulose.

© 2022 by the authors. This article is an open-access article distributed under the terms and conditions of the Creative Commons Attribution (CC BY) license (<https://creativecommons.org/licenses/by/4.0/>).

1. Introduction

Coir is a naturally occurring fiber from coconut husk, a renewable resource. In terms of physical characteristics and chemical content, coir fibers are similar to wood fibers. Coir fiber production globally totals 1.3 million tonnes annually, while more than 45 % of it is produced in India [1]. Furthermore, Pollachi Coir Cluster in the Coimbatore district, India alone, contributes about 13.8 % (81,200 MT) of total coir fiber production [2]. Only a partial portion of the coconut husk is being utilized for the fiber extraction and production of value-added products like yarn, rugs, geotextiles, etc. Although efforts are being made to expand the export

markets for coir and coir products, most coconut husk remains underused. The coir fiber industry primarily uses the fiber directly without any further processing. Coir fiber primarily consists of cellulose, hemicellulose, and lignin. The lignin component is entirely amorphous and could be utilized as a good source of energy generation [3, 4]. At the same time, cellulose is a natural polymer consisting of both amorphous and crystalline regions. Its high molecular weight makes the cellulose both strong and biodegradable. Cellulose has a wide range of potential applications in the field of environment, medicine, and engineering among biopolymers [5]. As a result, various underutilized bioresidues are evaluated for cellulose extraction, and in this study, coir fibers were used. These fibers have a high cellulose content and are available in large quantities in the region, which is an essential criterion for raw material. All the methods for cellulose extraction entail treating fibers in alkali/acid with slight modifications based on the availability of resources and the nature of the raw material. Every approach has its own benefits and downsides regarding cellulose quantity and quality (composition and final properties). Among the products developed from cellulose, nanocellulose has high applicability due to its unique properties.

Nanocrystalline cellulose (NCC) is a nano-scale material with a rod-like or spherical structure. It is one of the most advanced cellulose-based materials having a wide range of applications. NCC with rod/needle-like structures have diameters ranging from 5 nm to 30 nm and lengths from 100 nm to several μm . NCC also reported having better physicochemical and mechanical properties, such as more reactive hydroxyl groups, high surface area, crystallinity, and thermal stability. Also, NCC is known for its biodegradability and biocompatibility [6]. Many researchers have synthesized nanocellulose from a wide range of bioresources, which includes wheat straw [7], sugar palm fibre [8], sugarcane bagasse [9], rice straw [10], groundnut shell [11], and sago seed shell [12].

Coir fiber, a lignocellulosic material with high cellulose content, could also synthesize nano-scale resources, such as nanocellulose fibrils/ nanocellulose whiskers/ nanocellulose crystals; only a few studies have reported nanocellulose production from coir fiber. [13] synthesized rod-like nanocrystals with a diameter ranging from 10 to 30 nm from the coir fiber through sulphuric acid hydrolysis. Similarly, nitric acid isolated cellulose nanowhiskers having 80 to 500 nm length and 6 nm width from the coconut husk fibers [14]. Nanocellulose fibrils isolated by [15] had a diameter of around 5-50 nm from the coir fiber through the steam explosion. Likewise, the alkali-acid hydrolysis method obtained 25 g of nanofibrils with 16 % cellulose content from 100 g of coir fiber [16]. However, these studies were conducted to maximize the yield of nanocellulose, while cellulose content in the synthesized nanomaterial was the least concern. Along with quantity, the quality of nanocellulose is also important for commercialization and successful application in various fields. Hence, this research aims to comprehensively explore efficient cellulose extraction through two techniques (steam explosion versus alkali-acid hydrolysis) and improve the process parameters for synthesizing high-quality nanocrystalline cellulose. Nanocellulose is a popular topic in current research [17–19], and its production using a low-cost technology and efficient use of nanocellulose for pollutant removal makes this study even more essential in the present-day environmental scenario.

2. Materials and Methods

2.1. Raw materials.

Coconut husk fibers were collected from the coconut processing farms located at Pollachi, Tamil Nadu, India (10.6609° N, 77.0048° E). The town of Pollachi, located in the shadows of the Western Ghats, provides ideal circumstances for the growth of coconut trees, which cover an area of around 50,000 hectares [2]. 30 million nuts were being produced, yielding 5 million tonnes of coconut husk each year.

2.2. Compositional analysis of coir fiber

Coir fiber was washed with water to remove the dust particles adhered to its surface, shade-dried for 48 h, and shredded into small fibers. The dried powder was used for compositional analysis. The amount of moisture, lignin, volatile matter and ash content was determined by following NREL procedures [20]. The carbon, hydrogen, and nitrogen were determined using CHNS analyzer Elementar Vario EL III equipment, Germany. The alpha-cellulose content was estimated using the standard procedure given by [21].

2.3. Extraction of cellulose from coir fiber.

2.3.1. Steam explosion method.

2.3.1.1. Delignification (Alkali treatment and bleaching).

Cellulose extraction is a two-step process *viz.*, pretreatment with alkali and delignification. Coir fibers were soaked in 2 % NaOH for 2 h at a temperature of 25 °C. It is known that the alkaline delignification process converts solid biomass lignin into a soluble liquid phase. Initially, steam pretreatment was performed by autoclaving the alkali-treated fiber at high pressure (20 lbs) and temperature (121 °C) for 1.5 h. This was followed by bleaching with sodium hypochlorite (NaClO) for 20 minutes to remove the residual lignin. The solution pH was maintained at 3.5 with 1 M glacial acetic acid. The bleached fibers were washed thoroughly with water to remove the traces of chlorine. This process was repeated until the residue became white or ivory yellow.

2.3.1.2. Acid treatment followed by steam explosion.

The delignified sample was then treated with 2 % oxalic acid, followed by the steam explosion at 20 lbs pressure and 121 °C for one hour. The acid-treated residue was then washed scrupulously until the wash water had neutral pH. The α -cellulose content was measured in the obtained residue.

2.3.2. Alkali-acid hydrolysis method.

2.3.2.1. Pretreatment and delignification.

The pretreatment was carried out by soaking the dried husk fibers in water for 3 h at 50 °C, followed by alkali treatment with 2 % NaOH at 80 °C for 3h (1 g/10 ml). After the delignification process, the fibers were washed repeatedly with distilled water until the wash water pH became neutral. The alkali-treated fibers were then oven-dried for 6 h at 80 °C,

followed by bleaching with sodium hypochlorite (pH – 3.5, adjusted with 1 M glacial acetic acid) for 20 min and washed several times with water to remove the traces of chlorine. This process was repeated until the residue became white or ivory yellow.

2.3.2.2. Alkali hydrolysis.

The bleached residue was treated with 0.05 N nitric acid at 70 °C for 1 h, followed by alkali hydrolysis with 0.1 M NaOH at 45 °C for 3 h. Then the substrate was washed with distilled water until the pH became neutral and dried in the oven at 80 °C for 3 h. The obtained cellulose is in the size range of 3-15 µm and was tested for its α-cellulose content.

2.4. Synthesis of nanocrystalline cellulose (NCC).

The cellulose obtained was subjected to concentrated acid hydrolysis with H₂SO₄. In general, the hydrolysis process needs 60 – 65 % concentrated sulphuric acid, 40 – 50 °C reaction temperature, and 30 – 60 min reaction time [22, 23]. As reported earlier, due to excessive degradation, the yield of synthesized NCC was very low (less than 30 wt%) [24]. Hence to overcome degradation, the range of reaction time, temperature, and acid concentration was widened [25] to obtain high-quality NCC.

2.4.1. Optimization of parameters for nanocellulose synthesis

Response Surface Methodology (RSM) is a statistical tool for designing experiments, assessing the influence of factors, and developing empirical models. The RSM tool reduces the trial runs needed to assess various factors and their interactions. The tests were designed and evaluated using the DESIGNEXPERT software (Stat-Ease, USA, version 13). In light of the results obtained from the previous studies, three factors, such as sulphuric acid concentration, reaction temperature, and hydrolysis time, were evaluated for their influence on nanocellulose synthesis using a box behken design. Each factor was fixed on three levels: sulphuric acid concentration (wt%) 45-65, time (min) 20-60, and temperature (°C) 40-60, and the response was cellulose content in NCC (Table 1), while corresponding NCC yield was also recorded. A total of 18 tests were performed as per the design. The model identified the expected ideal values of the factors using the point prediction method. Validation studies were carried out in triplicate under optimal conditions.

Table 1. Range of the factors used in box behken design for acid hydrolysis of cellulose.

Factors	Coded factor	Actual levels of coded factors		
		-1 (Low)	0 (Center)	+1 (High)
Acid concentration (wt%)	A	45	55	65
Reaction temperature (°C)	B	40	50	60
Hydrolysis time (min)	C	20	40	60

The acid hydrolysis was performed under continuous stirring conditions using a mechanical stirrer at 1200 rpm. A substantial amount of distilled water was added to the hydrolyzed cellulose to quench the reaction. To remove the excess sulphuric acid, the suspension was centrifuged for 20 min at 8,000 rpm and was dialyzed with distilled water. A constant pH was obtained in the dialyzed water after 2 days. Then to disperse the nanocrystals, the dialyzed NCC was suspended in distilled water at a 1:10 ratio and sonicated using probe

sonicator PR 250 for 20 min at 25-30 kHz. The obtained NCC was freeze-dried at -40 °C for 72 h and stored in a vacuum.

2.5. Characterization of NCC.

2.5.1. Morphological characterization.

The morphology of the samples was examined using Scanning electron microscopy (SEM) and Transmission electron microscopy (TEM). The Quanta 250 (FEI, Netherlands) scanning electron microscope was used to obtain SEM micrographs of the samples at different stages at a voltage of 10 kV. To eliminate the electron charging effects, the samples were coated with gold. TEM imaging was performed using FEI Techai Sprit (Netherlands) microscope with an accelerating voltage of 120 kV to study the nanostructure. Digital micrograph software was used to process the obtained images. Elemental analysis of the synthesized nanocellulose was studied using Energy dispersive x-ray (EDX) diffraction attached to the TEM unit.

2.5.2. Functional group analysis.

The surface functional groups of the synthesized nanocellulose were examined using Fourier-transform infrared spectroscopy (model 8400S of Shimadzu, Japan). The analysis was performed in the wavenumber range of 400 - 7000 cm^{-1} at 4 cm^{-1} resolution.

2.5.3. Crystallinity analysis.

The crystallinity degree of the samples was determined using an X-ray diffractometer (XPERT-PRO D8 Bruker) at 30 mA current and 40 kV voltage. The Cu K radiation ranged from 5° to 40°. The amorphous subtraction method was used to calculate the crystallinity index (X_c) by equation (1)

$$X_c = \frac{I_c - I_{am}}{I_c} \times 100 \quad \dots \dots (1)$$

where I_c and I_{am} are the peak intensities of crystalline and amorphous materials, respectively. The crystallite size was calculated by Scherrer equation (2)

$$\tau = \frac{K\lambda}{\beta \cos\theta} \quad \dots \dots (2)$$

where τ is the crystal dimension perpendicular to the diffracting planes with Miller Indices of hkl , λ is the wavelength of the X-ray radiation ($\lambda = 0.154 \text{ nm}$), β is the full width at half maximum (FWHM) of the diffraction peaks.

2.5.4. Thermal analysis

A thermogravimetric analyzer (TG/DTA - EXSTAR/6300) was used to evaluate the thermal stability of the samples. The heating rate was kept at 10 °C/min, and the temperature ranged from room temperature to 700 °C in the nitrogen atmosphere.

2.5.5. Zeta potential.

The surface charge of the nanocellulose sample was recorded by zeta potential using the instrument Horiba Scientific Nanopartica SZ-100 (Japan).

2.5.6. Determination of zero point charge (pH_{zpc}).

To determine the pH zero point charge of the synthesized NCC, the pH drift equilibrium technique was employed. Ten conical flasks, each containing 50 ml of 0.1 M NaCl, were taken, and the pH was adjusted from 2 to 12 using NaOH/H₂SO₄ solution. A known quantity of NCC was added to each flask, and the flasks were equilibrated for 24 h. The final pH was measured after 24 h. Change in pH was plotted against the initial pH, and the intersection point was taken as pH_{zpc} of the NCC.

2.6. Efficiency of synthesized nanocellulose as adsorbent for dyes.

The synthesized nanocrystalline cellulose was tested for its efficacy as an adsorbent for dyes. For this experiment, 2 cationic (Methylene blue (MB) and Crystal violet (CV)) and 2 anionic dyes (Congo red (CR) and methyl red (MR)) were taken. A 25 ml of each dye solution with 15 ppm initial concentration at different pH (5, 7, and 9) was prepared. The adsorbent dose, contact time, and rpm were fixed at 1g, 180 min, and 200 rpm, respectively. After the completion of the experiment, the amount of dye adsorbed was analyzed using a UV-Vis spectrophotometer (Thermoscientific Genesys 180). The maximum wavelength for the dyes methylene blue, crystal violet, methyl red, and congo red was obtained at 664, 586, 425, and 497 nm, respectively. The adsorption capacity (mg g⁻¹) of nanocellulose and the dye removal efficiency (%) was determined by the given formula.

$$\text{Dye removal efficiency (\%)} = \frac{C_0 - C_t}{C_0} \times 100 \quad \dots\dots (3)$$

$$\text{Adsorption capacity (mg g}^{-1}\text{)} = \frac{(C_0 - C_t) V}{M} \quad \dots\dots (4)$$

where C₀ is the initial dye concentration (mg L⁻¹), C_t is the dye concentration at time (mg L⁻¹), V is the volume of the dye solution (L), M is the weight of the adsorbent (g).

3. Results and Discussion

3.1. Compositional analysis of coir fiber.

The coir fiber was characterized by standard methods, and the results are shown in Table 2. Moisture, cellulose, hemicellulose, lignin, and ash content in the coir fiber were 9.30, 38.01, 2.30, 45.43, and 1.21 %, respectively. The presence of 38.01 wt% cellulose in coir fiber suggests that they could be used as a source for the extraction of cellulose [13]. These results are consistent with earlier coir fiber research [3, 4]. According to these authors, cellulose ranged from 23 to 43 percent, lignin from 35 to 54 percent, and ash from 1 to 3.5 percent, with the rest being extractive components. These values, on the other hand, are dependent on age, source, extraction duration, and process [3, 26]. Coir fiber has a 1.21 percent ash percentage, which is consistent with reported ranges of 1-3.5 percent [4]. When compared to other non-woody lignocellulosic materials, such as plantain stem (*Musa paradisiaca*) with a 55.80 percent ash content, coir fiber contains low extractives with little or no waxes and resin. Coir fiber consists of 46.75 % carbon, 5.41 % hydrogen, 0.91 % nitrogen, and 0.13 % sulfur. This is in

accordance with the results obtained by [27], who reported that coir fiber had 49.6 and 6.1 % carbon and hydrogen, respectively.

Table 2. Compositional analysis of coir fiber.

Parameters		Values
Proximate analysis (%)	Moisture content	9.30
	Ash content	1.21
Ultimate analysis (%)	Carbon	46.75
	Hydrogen	5.41
	Nitrogen	0.91
	Sulphur	0.13
Biochemical analysis (%)	Cellulose	38.01
	Hemicellulose	2.30
	Lignin	45.43

3.2. Extraction of cellulose (steam explosion vs. alkali-acid hydrolysis).

To obtain high-purity cellulose, effective pretreatment techniques are required to remove other components from the recalcitrant biomass, such as hemicellulose, lignin, and other extractives. In this study, delignification (alkali treatment) could have eliminated a significant percentage of lignin, as NaOH is best known to dissolve undesirable compounds in the fiber, so cellulose can be extracted [28]. Similarly, [29] also stated that the alkaline delignification method is known to convert solid biomass lignin into a soluble liquid phase. Furthermore, alkali concentration, reaction time, and temperature all influence lignin removal. In this study, the reduction percentage of lignin was higher in the hydrolysis method (95.6 %) than in the steam explosion (27.5 %). Accordingly, many studies have reported that 85 percent of lignin could be removed by treating lignocellulosic biomass with liquid at a higher temperature [30]. In the alkali-acid hydrolysis method, the duration and temperature of alkali treatment were higher than the steam explosion, which could have been the reason for the higher removal of lignin. Similarly, [31] reported that treatment with 2 % NaOH reduced the lignin content from 31 to 3 %.

To enhance the delignification, oxidizing agents are used after the pretreatment with alkali. In this study, sodium hypochlorite was used as the bleaching agent, a strong oxidant. Bleaching with oxidation agents could remove the lignin aggressively from the biomass. While under this mild condition, cellulose is hardly decomposed [32]. In accordance with this, bleaching combined with alkali treatment would have removed the remaining alkali-soluble lignin, hemicelluloses, and other impurities, thereby enhancing the cellulose percentage. [33] reported an increase in cellulose content from 45.9 to 62.8 % after bleaching the green coconut fiber with sodium hypochlorite. Among the two different methods tested for isolation, alkali-acid hydrolysis yielded the maximum cellulose content of 80.32 % w/w than the steam explosion (45.52 % w/w). Conversely, [15] reported higher cellulose content of 88.3 % in the steam-exploded cellulose fibrils. It could be due to the high cellulose content (40 %) in the raw coir fiber and the inclusion of a steam gun to extract cellulose. Hence in this study, alkali-acid hydrolysis is found to be suitable for extracting cellulose from coconut husk fiber. It was used for large-scale cellulose extraction from the fiber (Table 3).

Table 3. Constituents of coir fiber in different methods after extraction of cellulose.

S. No.	Parameters	Raw fiber	Physical method	Acid hydrolysis
1	Cellulose (%)	38.01	45.52	80.32
2	Hemicellulose (%)	2.30	1.51	<1
3	Lignin (%)	45.43	32.90	2.00

S. No.	Parameters	Raw fiber	Physical method	Acid hydrolysis
4	Moisture content (%)	9.30	10.20	8.10

3.3. Optimization of NCC synthesis.

The optimum conditions influencing NCC synthesis were determined using the Box Behnken design in response surface methodology. Acid concentration, reaction temperature, and hydrolysis time significantly affected the cellulose content in NCC. In run 10 (45 % acid @ 50 °C for 60 min), the synthesized NCC's maximum cellulose content of 85.61 percent was noted, compared to an expected value of 83 percent. To validate the appropriate values, the observed response was presented alongside the expected response (Table 4). The response surface is projected in contour plots, depicting the nature and magnitude of interaction among different factors. In contour plots, elliptical and circular nature indicated fairly prominent and insignificant interactions, respectively [34]. As per the earlier studies, the widened range of conditions should have resulted in NCC [35]. But we could observe denaturation of cellulose in trial runs 5, 14, 15, and 16 resulting in low NCC yield. Correspondingly, trial runs 9, 17, 8, 12, and 13 had the highest yield of NCC, whereas their cellulose content was found to be lower than 70 %. In contrast, the optimized process parameters yielded 19.7 g of NCC with 85.61 % highly desirable cellulose content. Similarly, the optimized process parameters for rice straw resulted in a synthesis efficiency of 90.28 % with a cellulose content of 89.2 % [36].

Table 4. Predicted and experimental responses of acid hydrolysis to synthesize NCC.

Run	A	B	C	Response (Cellulose content in NCC (%))		Corresponding NCC yield (g/100 g coir)
				Experimental	Predicted	
1	55	50	40	65.99	66.23	18.0
2	55	40	20	40.36	36.72	12.6
3	45	50	20	63.76	66.21	18.8
4	55	60	60	35.26	38.90	12.4
5	65	50	20	19.7	21.54	8.3
6	45	60	40	77.57	75.69	17.1
7	55	40	60	66.03	66.61	19.2
8	55	50	40	69.77	66.23	20.6
9	55	50	40	60.15	66.23	21.5
10	45	50	60	85.61	83.84	19.7
11	45	40	40	71.96	73.15	19.2
12	55	50	40	68.32	66.23	20.5
13	55	50	40	65.24	66.23	20.3
14	65	60	40	14.24	13.04	5.8
15	65	50	60	23.51	21.06	6.5
16	65	40	40	26.49	28.36	6.8
17	55	50	40	67.91	66.23	20.9
18	55	60	20	52.24	51.66	12.0

*A-Acid concentration (wt%), B-Reaction temperature (°C), C- Hydrolysis time (min)

3.3.1. Influence of acid concentration and reaction temperature on cellulose content of NCC.

A 3-D plot depicting the effect of reaction temperature and acid concentration on the cellulose content of NCC at the constant time (60 min) was shown in figure 1a. From the graph, it was revealed that cellulose content increases with a decrease in concentration and

temperature. Since high acid concentration could also solubilize cellulose via hydrolysis, an optimum acid content is required to ensure good cellulose recovery. In accordance with this, at a higher sulphuric acid concentration (65 wt%) and temperature (60 °C), the cellulose content of NCC was only 14.24 %, even though the reaction time was 40 min (Table 2). Nevertheless, cellulose content remained low, regardless of hydrolysis time at extreme acid concentration and temperature levels, demonstrating the importance of the acid concentration x temperature interaction. According to many previous studies, the typical concentration of sulphuric acid in the hydrolysis reaction for nanocellulose extraction is around 63 wt% [35]. But, the cellulose content was very low in the NCC obtained from the coir fiber at 65 % acid concentration. Similarly, hydrolysis with 63 % sulphuric acid resulted in 25 g of cellulose nanofibrils with 16 % cellulose content only [16]. Hence, low-concentration sulphuric acid hydrolysis for nanocellulose synthesis from coir fiber is appealing since it is more economical and environmentally friendly.

3.3.2. Influence of acid concentration and hydrolysis time on cellulose content of NCC.

The influence of acid concentration and hydrolysis time on the cellulose content of NCC at a constant temperature of 50 °C was illustrated in figure 1b. As hydrolysis time increases from 20 to 60 min, the cellulose content increases even at the low acid concentration. However, as acid concentration increases with time, the response begins to decrease. The higher acid concentration could have completely hydrolyzed the cellulose to simple sugars, and hence reduction in cellulose content in the synthesized NCC was observed. Similarly, [38] found that the nanocellulose quality and quantity could be significantly enhanced by increasing the reaction time while decreasing the acid concentration.

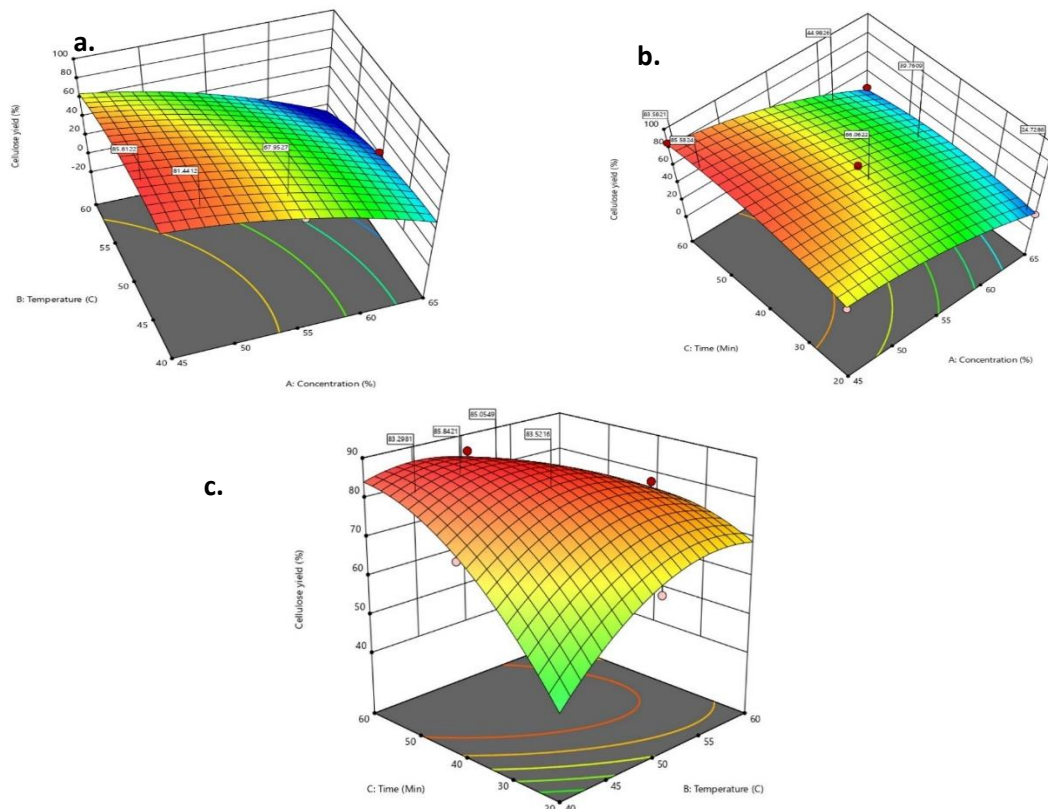


Figure 1. Contour plots. (a) Acid concentration (%) and reaction temperature (°C) at hydrolysis time 60 min; (b) Hydrolysis time (min) and acid concentration (%) at temperature 50°C; (c) Reaction temperature (°C) and hydrolysis time (min) at acid concentration 45 wt%.

3.3.3. Influence of reaction temperature and hydrolysis time on cellulose content of NCC

Figure 1c is a 3-D plot demonstrating the influence of reaction temperature and hydrolysis time on the cellulose content of NCC. It can be seen from the graph that cellulose content initially increases with an increase in the temperature and hydrolysis time when the acid concentration is at a minimum level (45 wt%). However, it began to decrease at temperatures above 50 °C. This decrease was caused by the complete hydrolysis of the cellulose into soluble sugars [37]. Also, the cellulose content showed decreasing trend when temperature and reaction time was at a minimum level. The lower reaction temperature and hydrolysis time could have caused insufficient hydrolysis, which led to lower cellulose content. The increasing temperature does not significantly improve the response as reaction time does. However, the reaction was difficult to control at 60 °C, and a color change was noticed after 15 min, indicating adverse reactions such as dehydration. The entire suspension had changed from white to black after 1 h at 60 °C. This is in line with the findings reported by [38]. He observed that the NCC yield at 56 wt% acids had no significant changes over different hydrolysis temperatures (50, 60, and 70 °C). Whereas, at long hydrolysis time with 56 wt% acid, the NCC yield was low due to the dissolution of cellulose. Hence, higher temperatures, longer reaction times, and low acid concentrations were found to yield high-quality nanocellulose.

3.4. Optimum process conditions and model verification.

The optimum conditions were found to be at 45 % (acid concentration), 50 °C (temperature), and 60 min (time). The cellulose content in the synthesized NCC is 85.6 %. The model's applicability for predicting the optimum response value was verified by comparing the experimental values with the predicted values obtained using the model equation. These experiments were conducted in triplicates, and the mean value of the cellulose content in NCC was calculated to be 86.12 %. We also found that 1 kg of dry raw coir fiber yielded 197 g of dry nanocellulose product.

3.5. Response surface methodology.

3.5.1. Model fitting.

The utilization of Design-Expert software led to the optimization of process parameters in order to achieve maximum quality in NCC. ANOVA (Analysis of variance) was carried out to analyze the experimental results, as shown in Table 5. The best-fitted model for optimizing cellulose content in NCC is a quadratic model. The model's F -value was 62.36, indicating that there is only a 0.01 percent probability that this value of F could occur due to experimental noise. This suggested that the model is significant and that all three factors (acid concentration, reaction temperature, and hydrolysis time) significantly influenced the response, as evidenced by the P -value of less than 0.05. The quadratic terms of the three factors were also shown to be significant. Interacting terms were likewise found to be significant, as seen by the 0.05 probability values [39]. As compared to pure error, "Lack of Fit" having F -value of 1.60 was found to be not significant. The coefficient of variation (CV) was also found to be 6.95 % from the ANOVA results, which according to [40] should not be larger than 10 %.

Similarly, the coefficient of determination (R^2) value of 0.98 was close to unity, indicating the empirical model's suitability to obtain experimental value [23]. This R^2 reflected

the amount of variation in the response that can be attributed to the model [41]. The predicted versus experimental values of cellulose content are given in Figure 2. The theoretical values are near the experimental values, indicating that the constructed model effectively links the correlation between the tested three factors and cellulose content in NCC. The developed model equation is:

$$\text{Yield (\%)} = 66.23 - 26.86A - 3.19B + 4.29C - 9.49A^2 - 9.18 B^2 - 8.58C^2 - 4.47AB - 4.53AC - 10.66BC$$

where A is the acid concentration (wt%), B is the hydrolysis time (minutes), and C is the reaction temperature (°C). Synergistic effects are represented by a positive sign, while a negative sign represents antagonistic effects. Overall, it can be concluded that this model was suitable for predicting the influence of three factors (acid concentration, reaction temperature, and hydrolysis time) on nanocellulose synthesis.

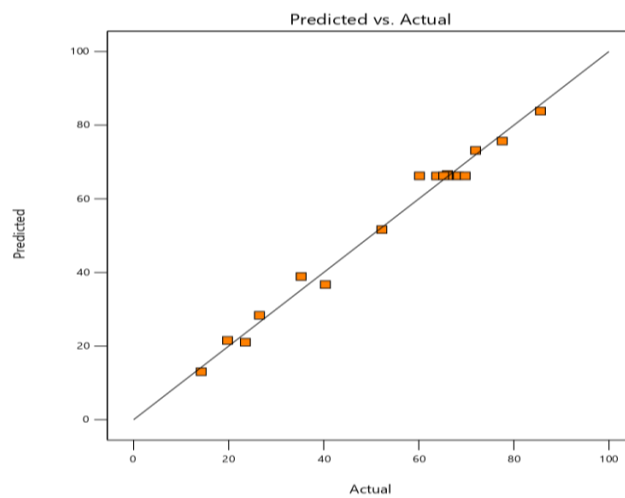


Figure 2. Predicted vs. actual response values.

Table 5. ANOVA for Quadratic model.

Source	Sum of Squares	df	Mean Square	F-value	p-value	
Model	7938.33	9	882.04	62.36	< 0.0001	Significant
A	5771.84	1	5771.84	408.07	< 0.0001	
B	81.52	1	81.52	5.76	0.0431	
C	146.93	1	146.93	10.39	0.0122	
AB	79.76	1	79.76	5.64	0.0449	
AC	81.95	1	81.95	5.79	0.0427	
BC	454.80	1	454.80	32.15	0.0005	
A ²	392.87	1	392.87	27.78	0.0008	
B ²	367.76	1	367.76	26.00	0.0009	
C ²	321.09	1	321.09	22.70	0.0014	
Residual	113.15	8	14.14			
Lack of Fit	55.37	3	18.46	1.60	0.3015	Not significant
Pure Error	57.78	5	11.56			
Cor Total	8051.48	17				
CV = 6.95 %	R ² = 0.98		Adj R ² = 0.97		Pred R ² = 0.87	

*A-Acid concentration (wt%), B-Reaction temperature (°C), C-Hydrolysis time (min)

3.5.1. Perturbation plot.

The perturbation plot is used to evaluate which numerical factor is the most sensitive to response and analyze each factor's effect on the response. By comparing the effect of all elements at a specific point, the reaction has been shown by changing only one component while the others remain constant. The behavior of each factor is studied to see how the response varies as it moves away from a specified reference point [42]. In a reaction, a curve or steep slope indicates how sensitive the response is to that factor, whereas a flat line indicates how insensitive the response is to that factor [43]. As illustrated in figure 3, the perturbation graph was plotted for all components in this study. The reference point for each factor was chosen in the middle of its range. The response was plotted against the set reference point after modifying the range of each individual element. The perturbation graph shows that component A has a steep slope and factors B and C have curvature, implying that the response (cellulose content in NCC) is sensitive to all three process parameter changes.

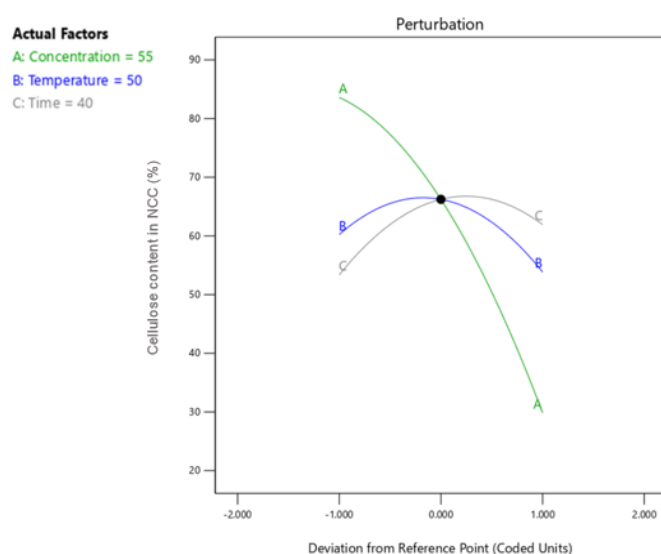


Figure 3. Perturbation plot depicting the effect of all factors on response.

3.6. Characterization of NCC.

3.6.1. Morphology by SEM and TEM.

Scanning with electron microscopy is a technique for obtaining high-resolution surface images. Figure 6a shows that the coir fiber had diameters ranging from 55 to 150 μm with a smooth surface due to the presence of some non-fibrous components such as lignin and waxes and had lesser pore size (Figure 4a). The lignin and hemicellulose were bleached off, and the fiber bundles were separated into individual cellulose microfibrils, as seen in Figure 4b. The diameter of extracted cellulose fibrils obtained after alkali hydrolysis was 2-3 μm (Figure 4c). Due to the hemicellulose degradation and partial lignin degradation caused by the repeated alkali treatment and bleaching, the surface of the cellulose microfibril exhibited an irregular porous structure.

Sulphuric acid hydrolysis individualized the cellulose microfibrils into numerous nano-sized crystals, as shown in the TEM micrograph (Figure 5a). Additionally, the TEM images revealed that the nanocellulose synthesized was distinct from the typical needle- or rod-like morphologies of nanocrystal cellulose [44].

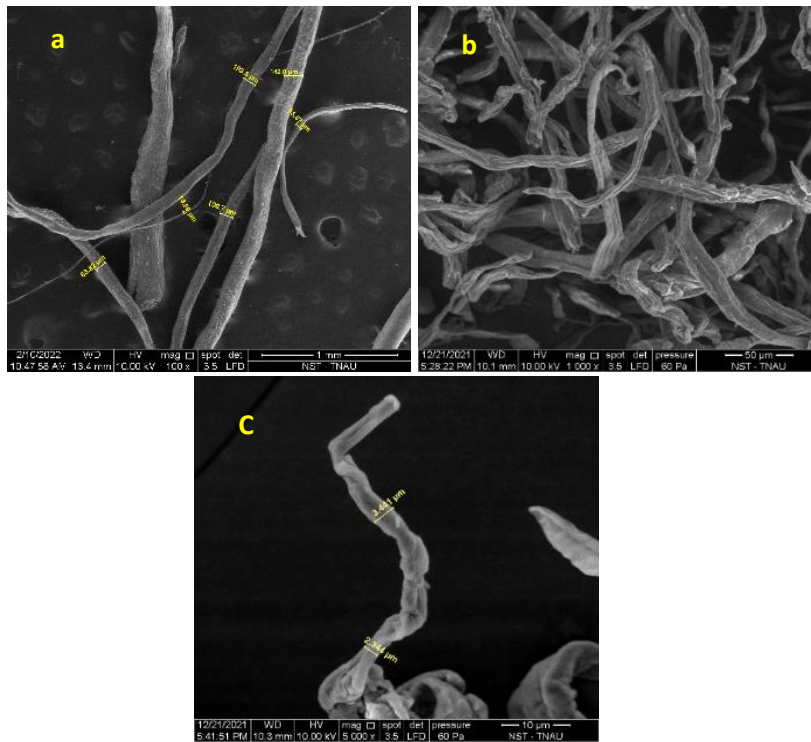


Figure 4. SEM micrographs (a) Coir fibre; (b) Cellulose after alkali hydrolysis; c. Individual cellulose microfibril.

The spherical nanocrystals had diameters below 40 nm. Nanocellulose dimensions strongly depend on the hydrolysis conditions and extraction techniques [45]. In this study, sulphuric acid could have removed the amorphous region in the extracted cellulose by causing the hydrolytic cleavage of glycosidic bonds. The properties of nanocelluloses, such as optical characteristics, stability, and rheology in aqueous conditions, influence their size and shape, as has been described [46], and these properties significantly determine the application of nanocellulose. The NCC's size dimensions indicate that they will be ideal templates for making nanocomposites, which enhances their mechanical properties and speed up their biodegradability [47]. Especially, the spherical or square structures of nanocellulose make them suitable for emulsion stabilizers [48] or as drug delivery carriers for encapsulation [49]. Also, when nanocellulose is used in paper making, it increases density while decreasing the opacity and roughness of the paper [50].

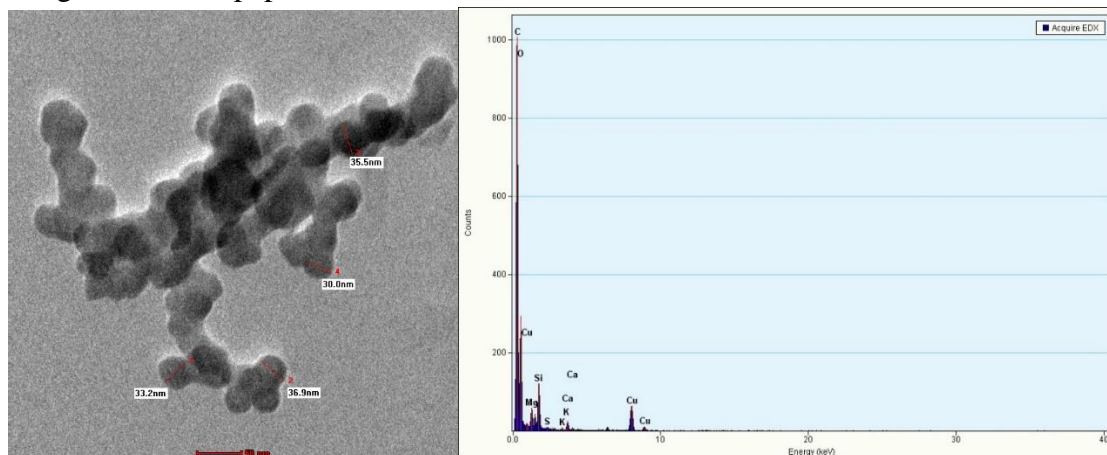


Figure 5. (a) TEM micrograph of synthesized spherical nanocellulose; (b) EDX spectrum of synthesized nanocellulose.

For elemental analysis of NCCs, energy dispersive x-ray diffraction (EDX) attached with TEM was employed. According to their respective binding energies, carbon, oxygen, calcium, copper, and sulfur peaks were evident in the EDX spectrum (Figure 5b). This elemental impurity (sulfur) resulted from the cellulose fibers being hydrolyzed by H₂SO₄ acid, while copper was due to the grid in which the samples were placed for analysis. [51] also reported 0.72 % sulfur along with oxygen (56.12 %) and carbon (43.13 %) in the cellulose nanocrystals obtained from bagasse through acid hydrolysis.

3.6.2. Functional group characteristics by FTIR

The FTIR spectrum of synthesized nanocellulose showed distinct absorption patterns corresponding to each cellulose functional group (Figure 6). The spectra obtained from this study were in good covenant with previously reported cellulose spectra (Table 6). The raw coir fiber exhibited characteristic lignin peaks at 1229, 1505, and 1601 cm⁻¹ attributed to aromatic C–O–C stretching and C=C skeletal vibrations of the lignin compound [35, 52]. Also, the band at 1739 cm⁻¹ corresponds to the C=O stretching vibrations of acetyl and carboxyl groups of hemicellulose [13]. In the nanocellulose spectra, the peak was absent, indicating the removal of hemicellulose during the extraction process. In the nanocellulose sample, additional functional groups were also obtained, implying that new bonds were formed during acid hydrolysis. Sulphuric acid hydrolysis would have functionalized the sulfate groups on the NCC surface, improving their thermal stability and enabling them to be used as reinforcing agents in various thermoplastic matrixes [53].

Table 6. FTIR spectral bands of synthesized NCC.

S. No.	Spectral Bands	Wavenumber (cm ⁻¹)	
		Synthesized NCC	Reported cellulose
1.	C–H rock vibration	1029	905-1036
2.	C–O–C glycosidic band stretching vibration	1054	1162-1172
3.	CH ₂ bending vibration	1427	1425-1468
4.	H ₂ O absorbed	1630	1629-1645
5.	C–H stretching vibration	2890	2890-2900
6.	–OH groups stretching vibration	3330	3327-3450

In the nanocellulose spectra, the C-O stretching of cellulose is represented by the characteristic peak at 1029 cm⁻¹ and 1427 cm⁻¹, while the peak showed C-O stretching vibrations at 1054 cm⁻¹. Additionally, 898 cm⁻¹ and 1160 cm⁻¹ peaks attributed to the C-H deformations and C-O-C stretching vibrations of cellulose, respectively [54]. A sulfated group (SO₂) presence in the NCC spectrum was shown by the peak at 1160 cm⁻¹, which was most likely caused by cellulose sulfonation during the acid hydrolysis process with sulphuric acid [55]. The bands at 664 cm⁻¹ and 1630 cm⁻¹ correspond to the presence of C-OH out-of-plane bending in cellulose and OH bending due to absorbed water, respectively [56]. Also, acid hydrolysis exposed the hydroxyl groups of cellulose bound by intermolecular hydrogen bonding, which is exhibited by the broadband at 3330 cm⁻¹ as reported by [15] in his study. The strength and crystallinity of cellulose are determined by this inter- ((O(6)H---O(3')) and intra-molecular ((O(2)H---O(6) and O(3)H---O(5)) hydrogen bonding which was due to the presence of pendant hydroxyl groups [57]. The presence of hydroxyl groups in NCC could accelerate epoxy curing, which makes the NCC synthesized from coir fiber highly suitable for applications in emulsions. Therefore, the FTIR study revealed that the process of acid and alkali treatments reduced the quantum of binding components contained in the fibers.

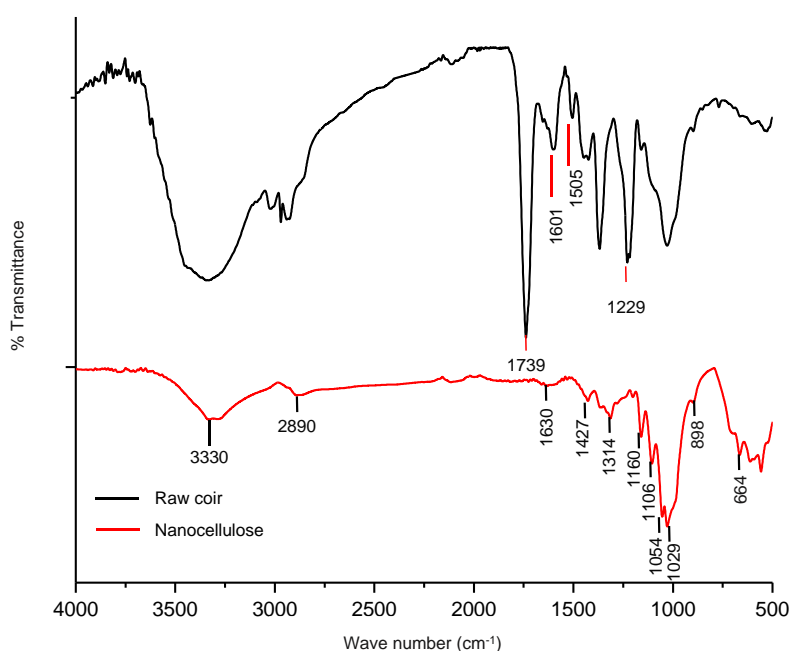


Figure 6. FTIR spectra of raw coir and nanocellulose.

3.6.3. Crystallinity analysis.

The crystalline properties of cellulose influence its mechanical and thermal properties [58]. The XRD diffraction patterns of synthesized nanocellulose were obtained at $2\theta = 16.6^\circ$, 22.6° , and 34.6° , which corresponds to the lattice planes 110, 200, and 004 in the cellulose lattice (Figure 7). The prominent crystalline peak at 22.6° with 100 % intensity confirmed the presence of crystalline nanocellulose. Specifically, cellulose crystallinity has been used to determine fiber elasticity, thermal stability, and absorption capacity, all key industrial application properties.

Components of nanocrystalline cellulose are embedded in a matrix of amorphous lignin, pectin, hemicellulose, and other elements in raw fiber. The matrix materials reacted with sodium hydroxide during alkali treatment and began to disintegrate. By defibrillating the fiber, the high temperature will make it easier for the alkali to get into the interior section of the raw coir. Figure 8 showed no crystalline peaks in the raw coir fiber because of the presence of amorphous lignin and hemicelluloses. A broad peak was observed at $2\theta = 15 - 19^\circ$ in the raw coir sample, which is associated with the overlapping of crystalline cellulose I to amorphous cellulose, hemicellulose, and lignin. It is clear from the graph that raw coir fibers can be categorized as lignocellulosic material [59]. Pretreatment with alkali and bleaching had removed these amorphous compounds and other impurities so that the crystallinity of NCC was increased to 80.05 % (calculated using Eq. 1). The increased crystallinity due to stronger molecular hydrogen bonding could explain the more pronounced peaks in these samples [60]. According to previous studies, the sulfate groups attached to the surface of NCC would give a negative charge leading to electrostatic repulsion among the individual nanocrystals. This helps form homogeneous and stable aqueous suspensions of NCC [56]. This implied that synthesizing NCCs via acid hydrolysis would influence the highly ordered crystallites by reducing hydrogen bond formation. The high crystallinity index of the NCC synthesized can thus be linked to the degree of hydrogen bonding and close packing. Sulphuric acid modification of cellulose resulted in well-orientated crystallites, as seen in the XRD graph in Figure 8. In line with the results, [13] also reported 78.55 percent crystallinity of NCC

synthesized from coir fiber by sulphuric acid hydrolysis. [61] has reported that acid hydrolysis with hydrochloric acid had increased the cellulose CI to 75 % from 43.45 % in raw coconut fiber. Cellulose extracted from Poplar wood chips (50 percent) [62], *Eucalyptus Bentharii* (54 percent), and *E. globulus* (55.3 percent) [63] had lower CIs than our value. The characterization of cellulose crystallinity is also confirmed by crystallite size. The crystallite size of the synthesized nanocrystalline cellulose was found to be 10.77 nm using Eq. 2. Similar to our results, [64] also obtained spherical nanocrystals from cotton waste with 7.44 nm crystallite size by sulphuric acid hydrolysis.

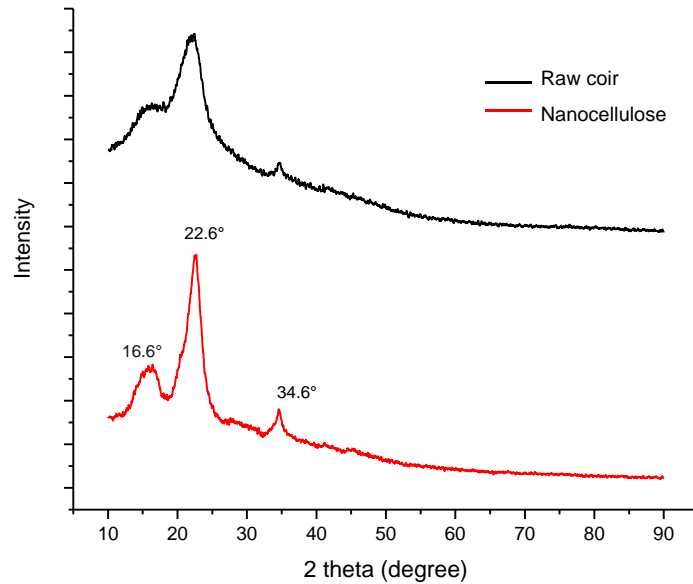


Figure 7. X-ray diffractogram of raw coir and nanocellulose.

3.6.4. Thermogravimetric analysis.

The TGA and DTG (Derivative thermogravimetry) curves of the raw coir fiber and synthesized nanocellulose are illustrated in Figure 8. In this study, raw coir fiber exhibited decomposition in stages, showing several components that decompose at variable temperatures. Because lignin, cellulose, and hemicellulose have different chemical structures, they typically degrade at various temperatures. In both samples, a small weight loss was observed from 40 to 100 °C due to moisture loss and low molecular weight compounds [65]. In this study, the nanocellulose was found to be thermally stable up to 193 °C.

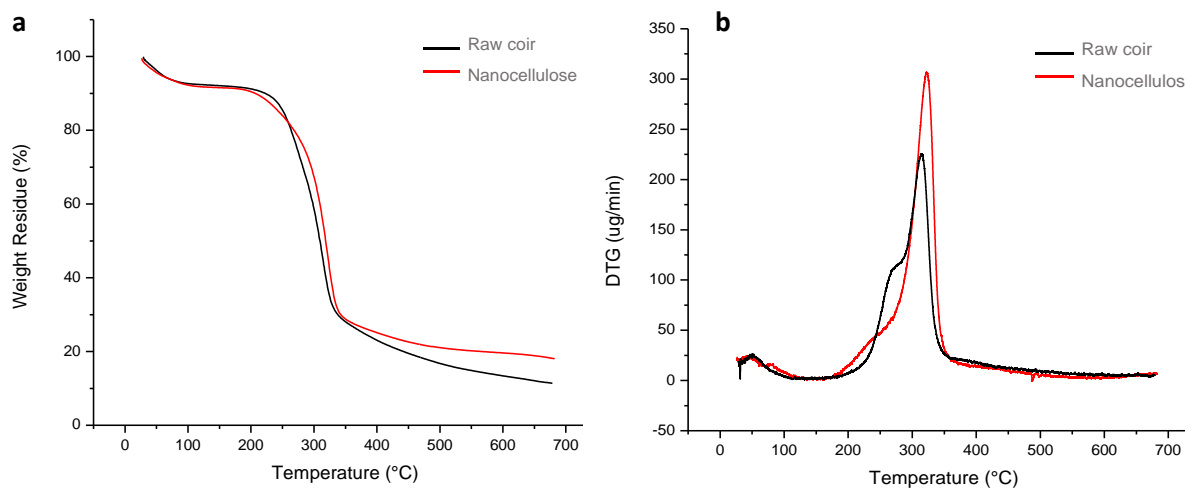


Figure 8. (a) TGA of raw coir and nanocellulose and (b) DTG of raw coir and nanocellulose.

Figure 8b shows that the decomposition of the primary cementing component, lignin started at 220 °C and attained its peak at 300 °C in the raw fiber [66]. The decomposition of lignin extended above 500 °C. Due to the presence of several chemical bonds in its structure, lignin breakdown is characterized by a wide temperature range [36]. In this instance, synthesized nanocellulose degrades at a lower temperature of 180 °C than the raw coir fiber (193 °C). As suggested in previous studies, this could be due to sulfate groups [67]. Additionally, sulphuric acid used in hydrolysis was thought to dissolve certain crystalline segments and remove non-crystalline segments. So, increasing temperature makes the material more prone to decomposition [12]. Also, the percent solid residue left after the pyrolysis was higher in the nanocellulose than in the raw coir. Hence, it can be concluded that better thermal stability has been linked to the partial removal of lignin and higher crystallinity of the cellulose [65].

3.6.5. Zeta potential.

The zeta potential measures the dispersibility of the nanomaterial, with a higher absolute value implying greater dispersibility. In terms of absolute values, the zeta potential of NCC isolated from coir fiber (- 72.2 mV) was higher than ± 30 mV, the required threshold for electrostatic stability [68, 69]. This is most likely due to the sample's smaller average diameter size particles, which results in a decreased particle mass, leading to higher velocity movement and a larger zeta potential [70]. Another possible reason could be the presence of more negatively charged sulfate and carboxylic groups on the surface [71]. Similarly, [72] isolated cellulose nanowhiskers through sulphuric acid hydrolysis of cotton fibers and reported a high zeta potential of -69.7 mV due to the presence of sulfate groups on the surface. According to [71], NCC is prepared by hydrochloric acid hydrolysis aggregate due to the absence of electrostatic repulsive forces between the crystalline particles, which was not found in NCC synthesized by sulphuric acid hydrolysis. These findings corroborated with [73], in which they observed that the use of sulphuric acid rather than hydrochloric acid lowers the potential for starch nanocrystal agglomeration and prevents their flocculation in aqueous conditions. Many nanomaterials with high zeta potential values of NCC, as high as -58 mV to -25 mV [9, 74], were obtained through sulphuric acid hydrolysis. Modifying surface charges of nanocellulose after synthesis based on their zeta potential could be used to remove specific pollutants or compounds from the environment [75].

3.6.5. Zero point charge (pH_{zpc}).

The surface charge of the adsorbent material in an aqueous solution is characterized by the zero point charge. The pH_{zpc} of the cellulose-chitosan hydrogel beads was found to be 7.00 (Figure 9). The surface charge of the adsorbent material in an aqueous solution is characterized by the zero point charge. The pH_{zpc} of the cellulose-chitosan hydrogel beads was found to be 7.00. Thus, the surface charge of the adsorbent is neutral at this pH ($\text{pH} = 0$). Due to the electrostatic forces favoring cation adsorption, the surface of the adsorbent becomes negatively charged when $\text{pH} > \text{pH}_{\text{zpc}}$, whereas when $\text{pH} < \text{pH}_{\text{zpc}}$, it attains a positive charge as the adsorption of H^+ occurs [76].

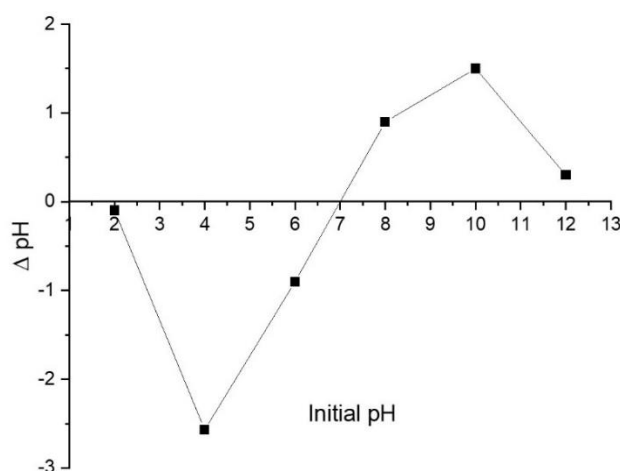


Figure 9. Zero point charge (pHzpc) of the synthesized NCC.

3.7. Adsorption of dyes by the synthesized NCC.

Based on the morphology and physicochemical properties of the NCCs, dyes might be adsorbed and/or trapped in the porous structures on the surface. Among the 4 dyes, the removal efficiency of NCC was higher for methylene blue (Table 7). In this study, methylene blue removal and NCC adsorption capacity remained almost the same at 90 % and 0.71 mg g⁻¹, respectively, despite the pH increase. But, [77] reported that nanocellulose isolated from the kenaf core had removed a higher percentage (80 %) of methylene blue at alkaline pH than the acidic pH (35 %). Adsorbent surface charges are affected by the solution pH by protonating or deprotonating the functional groups [78]. However, in the case of adsorbents containing functional groups such as -COO-, -OSO₃-, the negative surface charge decreased when pH approached the pKa of the functional groups. The FTIR results show that synthesized NCC had sulfate groups that have pKa around 1.9. Because of this, methylene dye removal percentages between pH 5 to 9 were not affected. In a similar manner, congo red removal percentage also remained unchanged (87-89 %) at different pH levels. This experiment found that electrostatic interaction between the adsorbent and the dyes (MB and CR) played a greater role than the pH of the solution.

Table 7. Removal efficiency (%) and dye adsorbed (mg g⁻¹) by the synthesized NCC at different pH.

Dyes	Initial concentration	pH	Removal Efficiency (%)	Dye adsorbed - q _t (mg g ⁻¹)
Methyl Red	15 ppm	5	52.86	0.40
		7	57.38	0.44
		9	43.10	0.33
Congo Red	15 ppm	5	87.74	0.84
		7	89.29	0.86
		9	89.96	0.87
Methylene Blue	15 ppm	5	90.82	0.71
		7	90.89	0.71
		9	90.86	0.71
Crystal Violet	15 ppm	5	72.45	0.54
		7	75.85	0.57
		9	79.18	0.59

Interestingly, the adsorption capacity of NCC for crystal violet had increased from 0.54 to 0.59 mg g⁻¹ with increasing pH from 5 to 9. Higher removal percentage (79.18 %) of crystal violet was observed at alkaline pH of 9. As the pHzpc of synthesized nanocellulose is 7.00, the adsorbent surface is negatively charged above 7.00 due to increased deprotonation of amine

groups, *i.e.*, NH_2 , on the adsorbent. This explained the higher removal of crystal violet at higher pH. Moreover, higher pH values ($\text{pH} > 7$) allow the NCC surface to be negatively charged, which is conducive to cationic dyes being associated with adsorbents [79]. The lower CV adsorption at acidic pH values is probably due to excess H^+ ions competing with dye cations for adsorption sites. Among the dyes, the lowest adsorption by NCC was observed for methyl red. The adsorption capacity of NCC and removal percentage was higher in neutral pH (7) with 0.44 mg g^{-1} and 57.38 %, respectively. The removal percentage was low at the alkaline pH (43.1 %) than at the acidic pH (52.86 %). Methyl red being an anionic dye, its adsorption onto NCC was favored at pH below pH_{zpc} . This could be due to the increased H^+ ions leading to higher protonation on the adsorbent surface and increased electrostatic attraction between the anionic dye and positively-charged NCC. These results suggest that synthesized NCC can be used for removing dyes from textile effluents in a wide pH range.

3.8. High-value NCC synthesis cost.

Coconut husk fiber is a predominant residue in coconut cultivation and its allied industrial sectors. The fiber is used to produce coir yarn and geotextiles, which have a niche market in the local area. The cost of coir fiber, coir yarn, and geotextile (A grade) are 13, 38, and 70 Rupees (INR) per kg, which draw marginal profits due to the high cost of skilled labor [80]. Hence, an alternative product with wide applications could help the thriving sector amidst the demand for skilled labor. Nanocrystalline cellulose price varies from Rs. 10,000 to an astounding price of 1.6 lakhs per kg based on its source for raw material, processing method, properties, and numerous applications [81, 82]. Hence, the cost of extracting the NCC in this study could help us understand the economic viability of large-scale extraction of nanocellulose (Table S1). Five kilograms of raw coir fiber procured for Rs. 65 was utilized to extract one kilogram of NCC [80]. The acids and alkali used in this extraction cost around Rs. 6857 (Unpublished price list obtained through tender), which could be reduced when purchased at a large scale. The electricity cost was around Rs. 105.60. The unsorted materials and water utilized in this extraction process are valued at around Rs. 2139 in the region. Hence, the total processing cost for extracting one kilogram of NCC is Rs. 9166 (INR). While the cost of infrastructure, labor, and capital investments holds the lion's share, it is excluded from the cost of extracting NCC in this study since it was carried out on a laboratory scale. However, pilot scale studies are required to ascertain the capital cost and actual production potential. Based on the current assessment, extraction of high-value NCC from coconut fibers is an economically viable alternative to existing technological interventions.

4. Conclusions

This study's objective was to synthesize nanocellulose from raw coir fiber to enhance its efficient use in various applications. The extraction of nanocellulose from raw coir fiber has been found to be successful *via* alkali-acid hydrolysis. Alkali-acid hydrolysis method produced homogeneous spherical nanocrystals from coir fiber with a diameter below 40 nm under optimized conditions (45 % acid @ 50 °C for 60 min). However, the efficiency of cellulose extraction from coir fiber was reported to be 50-60 % with existing technologies. Hence, improvement in the efficiency of the process with further research with technological advancements would be the way forward. Since pure cellulose has a wide range of properties, its nano form can be used in various industrial and biological arenas by integrating

nanotechnology. Furthermore, as demonstrated in this study, the synthesized NCC could be efficiently used to remove various dyes from the textile and dyeing effluents. Surface modification of NCC during synthesis would improve its potential to remove a wide variety of pollutants.

Funding

This research received no external funding.

Acknowledgments

The authors thank Tamil Nadu Agricultural University, Coimbatore, for providing all resources for performing the research and the Department of Science and Technology, Science and Engineering Research Board (DST-SERB) for their financial support (EEQ/2016/000807).

Conflicts of Interest

The authors declare no conflict of interest.

References

1. FAOstat Crops and Livestock Products <https://www.fao.org/faostat/en/#data/QCL>.
2. Coir Board. DETAILED PROJECT REPORT Cluster Location: POLLACHI, COIMBATORE DISTRICT. **2016**, Available online: <http://coirboard.gov.in/wp-content/uploads/2016/03/FINAL-ECO-Coir-Pollachi-Writeup1.pdf>.
3. Narendar, R.; Priya Dasan, K. Chemical Treatments of Coir Pith: Morphology, Chemical Composition, Thermal and Water Retention Behavior. *Compos. Part B Eng.* **2014**, *56*, 770–779, <https://doi.org/10.1016/j.compositesb.2013.09.028>.
4. Barbosa, V.; Ramires, E.C.; Razera, I.A.T.; Frollini, E. Biobased Composites from Tannin-Phenolic Polymers Reinforced with Coir Fibers. *Ind. Crops Prod.* **2010**, *32*, 305–312, <https://doi.org/10.1016/j.indcrop.2010.05.007>.
5. Huntley, C.J.; Crews, K.D.; Abdalla, M.A.; Russell, A.E.; Curry, M.L. Influence of Strong Acid Hydrolysis Processing on the Thermal Stability and Crystallinity of Cellulose Isolated from Wheat Straw. *Int. J. Chem. Eng.* **2015**, *2015*, <https://doi.org/10.1155/2015/658163>.
6. Banza, M.; Rutto, H. Extraction of cellulose nanocrystals from millet (*Eleusine coracana*) husk waste: optimization using Box Behnken design in response surface methodology (RSM). *Int Nano Lett.* **2022**, *12*, 257–272, <https://doi.org/10.1007/s40089-022-00369-x>.
7. Nehra, P.; Chauhan, R.P. Facile synthesis of nanocellulose from wheat straw as an agricultural waste. *Iran Polym J.* **2022**, *31*, 771–778, <https://doi.org/10.1007/s13726-022-01040-0>.
8. Ilyas, R.A.; Sapuan, S.M.; Ishak, M.R. Isolation and Characterization of Nanocrystalline Cellulose from Sugar Palm Fibres (*Arenga Pinnata*). *Carbohydr. Polym.* **2018**, *181*, 1038–1051, <https://doi.org/10.1016/J.CARBPOL.2017.11.045>.
9. de Morais Teixeira, E.; Corrêa, A.C.; Manzoli, A.; de Lima Leite, F.; de Ribeiro Oliveira, C.; Mattoso, L.H.C. Cellulose Nanofibers from White and Naturally Colored Cotton Fibers. *Cellul.* **2010**, *17*, 595–606, <https://doi.org/10.1007/S10570-010-9403-0>.
10. Lu, P.; Hsieh, Y. Lo Preparation and Characterization of Cellulose Nanocrystals from Rice Straw. *Carbohydr. Polym.* **2012**, *87*, 564–573, <https://doi.org/10.1016/J.CARBPOL.2011.08.022>.
11. Bano, S.; Negi, Y.S. Studies on Cellulose Nanocrystals Isolated from Groundnut Shells. *Carbohydr. Polym.* **2017**, *157*, 1041–1049, <https://doi.org/10.1016/J.CARBPOL.2016.10.069>.
12. Naduparambath, S.; Purushothaman, E. Sago Seed Shell: Determination of the Composition and Isolation of Microcrystalline Cellulose (MCC). *Cellul.* **2016**, *23*, 1803–1812, <https://doi.org/10.1007/S10570-016-0904-3>.
13. Ikhuoria, E.; Omorogbe, S.; Agbonlahor, O.; Etiuma, R. Nanocellulose Crystals from Coir Fibre for Template Application. *Am. Chem. Sci. J.* **2015**, *9*, 1–11, <https://doi.org/10.9734/acsj/2015/18766>.

14. Rosa, M.F.; Medeiros, E.S.; Malmonge, J.A.; Gregorski, K.S.; Wood, D.F.; Mattoso, L.H.C.; Glenn, G.; Orts, W.J.; Imam, S.H. Cellulose Nanowhiskers from Coconut Husk Fibers: Effect of Preparation Conditions on Their Thermal and Morphological Behavior. *Carbohydr. Polym.* **2010**, *81*, 83–92, <https://doi.org/10.1016/j.carbpol.2010.01.059>.
15. Abraham, E.; Deepa, B.; Pothen, L.A.; Cintil, J.; Thomas, S.; John, M.J.; Anandjiwala, R.; Narine, S.S. Environmental Friendly Method for the Extraction of Coir Fibre and Isolation of Nanofibre. *Carbohydr. Polym.* **2013**, *92*, 1477–1483, <https://doi.org/10.1016/j.carbpol.2012.10.056>.
16. Rojas-Valencia, M.N.; Galeana-Olvera, E.; Y. Fernández-Rojas, D.; Mendoza-Buenrostro, C.; Nájera-Aguilar, H.A.; Vaca-Mier, M. Isolation of Cellulose Nanofibrils from Coconut Waste for the Production of Sewing Thread. *Adv. Mater. Sci.* **2018**, *3*, 1–3, <https://doi.org/10.15761/ams.1000135>.
17. Zhu, P.; Feng, L.; Ding, Z.; Bai, X. Preparation of Spherical Cellulose Nanocrystals from Microcrystalline Cellulose by Mixed Acid Hydrolysis with Different Pretreatment Routes. *Int. J. Mol. Sci.* **2022**, *23*, 10764. <https://doi.org/10.3390/ijms231810764>.
18. Collazo-Bigliardi, S.; Ortega-Toro, R.; Chiralt Boix, A. Isolation and Characterisation of Microcrystalline Cellulose and Cellulose Nanocrystals from Coffee Husk and Comparative Study with Rice Husk. *Carbohydr. Polym.* **2018**, *191*, 205–215, <https://doi.org/10.1016/J.CARBPOL.2018.03.022>.
19. Trache, D.; Tarchoun, A.F.; Derradji, M.; Hamidon, T.S.; Masruchin, N.; Brosse, N.; Hussin, M.H. Nanocellulose: From Fundamentals to Advanced Applications. *Front. Chem.* **2020**, *8*, 392, <https://www.frontiersin.org/articles/10.3389/fchem.2020.00392/full>.
20. Anisuzzaman, S.M.; Fong, Y.W.; Madsah, M. A Review on Various Techniques and Recent Advances in Polymeric Additives to Mitigate Wax Problems in Crude Oil. *J. Adv. Res. Fluid Mech. Therm. Sci.* **2018**, *48*, 53–64, <https://www.akademiabaru.com/submit/index.php/arfmts/article/view/2259>.
21. Updegraff, D.M. Semimicro Determination of Cellulose Inbiological Materials. *Anal. Biochem.* **1969**, *32*, 420–424, [https://doi.org/10.1016/S0003-2697\(69\)80009-6](https://doi.org/10.1016/S0003-2697(69)80009-6).
22. Pandey, J.K.; Takagi, H.; Nakagaito, A.N.; Kim, H.J. Handbook of Polymer Nanocomposites. Processing, Performance and Application: Volume C: Polymer Nanocomposites of Cellulose Nanoparticles. In Handbook of Polymer Nanocomposites. Processing, Performance and Application: Volume C: Polymer Nanocomposites of Cellulose Nanoparticles; Pandey, J.K., Takagi, H., Nakagaito, A.N., Kim, H.-J., Eds.; Springer-Verlag Berlin Heidelberg, **2015**; 15–26, <https://materials.springer.com/bp/docs/978-3-642-45232-1>.
23. Hassan, T.M.; Hossain, M.S.; Kassim, M.H.M.; Ibrahim, M.; Rawi, N.F.M.; Hussin, M.H. Optimizing the Acid Hydrolysis Process for the Isolation of Microcrystalline Cellulose from Oil Palm Empty Fruit Bunches Using Response Surface Methods. *Waste and Biomass Valorization* **2020**, *11*, 2755–2770, <https://doi.org/10.1007/s12649-019-00627-8>.
24. Bondeson, D.; Mathew, A.; Oksman, K. Optimization of the Isolation of Nanocrystals from Microcrystalline Cellulose by Acid Hydrolysis. *Cellulose* **2006**, *13*, 171–180, <https://doi.org/10.1007/s10570-006-9061-4>.
25. Ioelovich, M. Peculiarities of Cellulose Nanoparticles. *TAPPI J* **2014**, *13*, 45–52.
26. Mishra, L.; Basu, G. Coconut Fibre: Its Structure, Properties and Applications. In Handbook of Natural Fibres-Volume 1: Types, Properties and Factors Affecting Breeding and Cultivation.; Ryszard, K.M., Maria, M.-T., Eds.; Matthew Deans, **2020**; 1–26, <https://www.elsevier.com/books/handbook-of-natural-fibres/kozlowski/978-0-12-818398-4>.
27. Wang, W.; Huang, G. Characterisation and Utilization of Natural Coconut Fibres Composites. *Mater. Des.* **2009**, *30*, 2741–2744, <https://doi.org/10.1016/j.matdes.2008.11.002>.
28. Tang, T.K.; Lee, Y.Y.; Phuah, E.T.; Tan, C.P.; Kanagaratnam, S.; Wang, Y.; Cheong, L.Z.; Jamalullail, N.A.; Yap, K.L.; Lee, C.M.; et al. Response Surface Methodology Optimization Study on Corncob Pretreatment: Reduction of Sodium Hydroxide Usage and Enhancement in Pulpzyme HC Biobleaching Efficiency. *Food Res.* **2021**, *5*, 201–213, [https://doi.org/10.26656/fr.2017.5\(2\).490](https://doi.org/10.26656/fr.2017.5(2).490).
29. Mbakop, S.; Nthunya, L.N.; Onyango, M.S. Recent Advances in the Synthesis of Nanocellulose Functionalized-Hybrid Membranes and Application in Water Quality Improvement. *Processes* **2021**, *9*, 611, <https://doi.org/10.3390/pr9040611>.
30. Yan, L.; Pu, Y.; Bowden, M.; Ragauskas, A.J.; Yang, B. Physicochemical Characterization of Lignocellulosic Biomass Dissolution by Flowthrough Pretreatment. *ACS Sustain. Chem. Eng.* **2016**, *4*, 219–227, <https://doi.org/10.1021/acssuschemeng.5b01021>.

31. Abu-Thabit, N.Y.; Judeh, A.A.; Hakeem, A.S.; Ul-Hamid, A.; Umar, Y.; Ahmad, A. Isolation and Characterization of Microcrystalline Cellulose from Date Seeds (*Phoenix Dactylifera* L.). *Int. J. Biol. Macromol.* **2020**, *155*, 730–739, <https://doi.org/10.1016/j.ijbiomac.2020.03.255>.
32. Kargarzadeh, H.; Ioelovich, M.; Ahmad, I.; Thomas, S.; Dufresne, A. Methods for Extraction of Nanocellulose from Various Sources. *Handb. Nanocellulose Cellul. Nanocomposites* **2017**, 1–49, <https://doi.org/10.1002/9783527689972.ch1>.
33. Brígida, A.I.S.; Calado, V.M.A.; Gonçalves, L.R.B.; Coelho, M.A.Z. Effect of Chemical Treatments on Properties of Green Coconut Fiber. *Carbohydr. Polym.* **2010**, *79*, 832–838, <https://doi.org/10.1016/J.CARBPOL.2009.10.005>.
34. Chang, K.L.; Chen, X.M.; Wang, X.Q.; Han, Y.J.; Potprommanee, L.; Liu, J. yong; Liao, Y.L.; Ning, X. an; Sun, S. yu; Huang, Q. Impact of Surfactant Type for Ionic Liquid Pretreatment on Enhancing Delignification of Rice Straw. *Bioresour. Technol.* **2017**, *227*, 388–392, <https://doi.org/10.1016/j.biortech.2016.11.085>.
35. Wulandari, W.T.; Rochliadi, A.; Arcana, I.M. Nanocellulose Prepared by Acid Hydrolysis of Isolated Cellulose from Sugarcane Bagasse. *IOP Conf. Ser. Mater. Sci. Eng.* **2016**, *107*, <https://doi.org/10.1088/1757-899X/107/1/012045>.
36. Thakur, M.; Sharma, A.; Ahlawat, V.; Bhattacharya, M.; Goswami, S. Process Optimization for the Production of Cellulose Nanocrystals from Rice Straw Derived α -Cellulose. *Mater. Sci. Energy Technol.* **2020**, *3*, 328–334, <https://doi.org/10.1016/j.mset.2019.12.005>.
37. Gashaw, A. Bioethanol Production from Fruit Wastes and Factors Affecting Its Fabrication. *Int. J. Chem. Nat. Sci.* **2014**, *2*, 132–140, <https://www.semanticscholar.org/paper/Bioethanol-Production-from-Fruit-Wastes-and-Factors-Gashaw/ad3b4c31178be200f0d01be29fedceefa91f89ad>.
38. Chen, L.; Wang, Q.; Hirth, K.; Baez, C.; Agarwal, U.P.; Zhu, J.Y. Tailoring the Yield and Characteristics of Wood Cellulose Nanocrystals (CNC) Using Concentrated Acid Hydrolysis. *Cellulose* **2015**, *22*, 1753–1762, <https://doi.org/10.1007/s10570-015-0615-1>.
39. Akhabue, C.E.; Osubor, N.T. Optimization of Extraction of Microcrystalline Cellulose from Orange Peel Waste Using Response Surface Methodology. *Ife J. Sci.* **2017**, *19*, 227, <https://doi.org/10.4314/ijfs.v19i2.3>.
40. Daniel, W.W.; Cross, C.L. *Biostatistics: A Foundation for Analysis in the Health Sciences*; Wiley, **2018**.
41. Li, Y.; Jiang, L.; Sui, X.; Wang, S. Procedia Engineering Optimization of the Aqueous Enzymatic Extraction of Pine Kernel Oil by Response Surface Methodology. *Procedia Eng.* **2011**, *15*, 4641–4652, <https://doi.org/10.1016/j.proeng.2011.08.872>.
42. Nizamuddin, S.; Mubarak, N.M.; Tiripathi, M.; Jayakumar, N.S.; Sahu, J.N.; Ganesan, P. Chemical, Dielectric and Structural Characterization of Optimized Hydrochar Produced from Hydrothermal Carbonization of Palm Shell. *Fuel* **2016**, *163*, 88–97, <https://doi.org/10.1016/j.fuel.2015.08.057>.
43. Gottipati, R.; Ecocarb, G.; Rourkela, T. Application of Response Surface Methodology for Optimization of Cr (III) and Cr (VI). *Res. J. Chem. Sci.* **2012**, *2*, 40–48.
44. Kontturi, E.; Laaksonen, P.; Linder, M.B.; Gröschel, A.H.; Rojas, O.J.; Ikkala, O. Advanced Materials through Assembly of Nanocelluloses. *Adv. Mater.* **2018**, *30*, 1703779, <https://doi.org/10.1002/adma.201703779>.
45. Doan, T.K.Q.; Chiang, K.Y. Characteristics and Kinetics Study of Spherical Cellulose Nanocrystal Extracted from Cotton Cloth Waste by Acid Hydrolysis. *Sustain. Environ. Res.* **2022**, *32*, 1–14, <https://sustainenvironres.biomedcentral.com/articles/10.1186/s42834-022-00136-9>.
46. Salas, C.; Nypelö, T.; Rodriguez-Abreu, C.; Carrillo, C.; Rojas, O.J. Nanocellulose Properties and Applications in Colloids and Interfaces. *Curr. Opin. Colloid Interface Sci.* **2014**, *19*, 383–396, <https://doi.org/10.1016/j.cocis.2014.10.003>.
47. Nasir, M.; Hashim, R.; Sulaiman, O.; Asim, M. Nanocellulose: Preparation Methods and Applications. In *Cellulose-Reinforced Nanofibre Composites: Production, Properties and Applications*; Elsevier Ltd, **2017**; 261–276, <https://doi.org/10.1016/B978-0-08-100957-4.00011-5>.
48. Kasiri, N.; Fathi, M. Production of Cellulose Nanocrystals from Pistachio Shells and Their Application for Stabilizing Pickering Emulsions. *Int. J. Biol. Macromol.* **2018**, *106*, 1023–1031, <https://doi.org/10.1016/j.ijbiomac.2017.08.112>.
49. Qing, W.; Wang, Y.; Wang, Y.; Zhao, D.; Liu, X.; Zhu, J. The Modified Nanocrystalline Cellulose for Hydrophobic Drug Delivery. *Appl. Surf. Sci.* **2016**, *366*, 404–409, <https://doi.org/10.1016/j.apsusc.2016.01.133>.

50. Robles, E.; Labidi, J.; Halász, K.; Csóka, L. Key Issues in Reinforcement Involving Nanocellulose. In *Cellulose-Reinforced Nanofibre Composites: Production, Properties and Applications*; Woodhead Publishing, **2017**; 401–425, <https://doi.org/10.1016/B978-0-08-100957-4.00018-8>.
51. Kumar, A.; Negi, Y.S.; Choudhary, V.; Bhardwaj, N.K. Characterization of Cellulose Nanocrystals Produced by Acid-Hydrolysis from Sugarcane Bagasse as Agro-Waste. *J. Mater. Phys. Chem.* **2014**, *2*, 1–8, <http://pubs.sciepub.com/jmpc/2/1/1/>.
52. Zi-Qian, T.; Kobayashi, T.; Aht-Ong, D. Extraction of cellulose nanofibers from empty palm fruit bunches via mechanical defibrillation. *J. Met. Mater. Miner.* **2021**, *31*, 10–19, <https://doi.org/10.55713/jmmm.v31i3.1138>.
53. Börjesson, M.; Sahlin, K.; Bernin, D.; Westman, G. Increased Thermal Stability of Nanocellulose Composites by Functionalization of the Sulfate Groups on Cellulose Nanocrystals with Azetidinium Ions. *J. Appl. Polym. Sci.* **2018**, *135*, 45963, <https://doi.org/10.1002/app.45963>.
54. Duarte Urueña, G.; Ribeiro, K.C.; Prestes, E.; Pinheiro, L.A.; Carvalho, B.M. Extraction of Cellulose Nanocrystal from Multilayer Packaging Residues Composed of a Mixture of Eucalyptus and Pine Fibers. *Waste and Biomass Valorization* **2021**, *12*, 5763–5777, <https://doi.org/10.1007/S12649-021-01383-4>.
55. Shahi, N.; Wang, P.; Adhikari, S.; Min, B.; Rangari, V.K. Biopolymers fractionation and synthesis of nanocellulose/silica nanoparticles from agricultural byproducts. *ACS Sustainable Chem. Eng.* **2021**, *9*, 6284–6295, <https://doi.org/10.1021/acssuschemeng.0c09342>.
56. Matebie, B.Y.; Tizazu, B.Z.; Kadhem, A.A.; Prabhu, S.V. Synthesis of Cellulose Nanocrystals (CNCs) from Brewer's Spent Grain Using Acid Hydrolysis: Characterization and Optimization. *Journal of Nanomaterials*, **2021**, *2021*. <https://doi.org/10.1155/2021/7133154>.
57. Fan, M.; Dai, D.; Huang, B. Fourier Transform Infrared Spectroscopy for Natural Fibres. In *Fourier Transform - Materials Analysis; IntechOpen*, **2012**, <https://www.intechopen.com/chapters/37067>.
58. Trilokesh, C.; Uppuluri, K.B. Isolation and Characterization of Cellulose Nanocrystals from Jackfruit Peel. *Sci. Rep.* **2019**, *9*, 1–8, <https://doi.org/10.1038/s41598-019-53412-x>.
59. Risite, H.; Salim, M.H.; Oudinot, B.T.; Ablouh, E. houssaine; Joyeux, H.T.; Sehaqui, H.; Razafimahatratra, J.H.A.; Qaiss, A.E.K.; El Achaby, M.; Kassab, Z. Artemisia Annuua Stems a New Sustainable Source for Cellulosic Materials: Production and Characterization of Cellulose Microfibers and Nanocrystals. *Waste and Biomass Valorization* **2022**, *13*, 2411–2423, <https://link.springer.com/article/10.1007/s12649-021-01658-w>.
60. Shaikh, H.M.; Anis, A.; Poulose, A.M.; Al-zahrani, S.M.; Madhar, N.A.; Alhamidi, A.; Alam, M.A. Isolation and Characterization of Alpha and Nanocrystalline Cellulose from Date Palm (Phoenix Dactylifera L.) Trunk Mesh. *Polymers (Basel)*. **2021**, *13*, 1893. <https://doi.org/10.3390/polym13111893>.
61. Nasution, H.; Harahap, H.; Suherman, P.; Kelvin Isolation and Characterization of Microcrystalline Cellulose from Coconut Fiber Using Acid Hydrolysis Process. In *Proceedings of the International Conference of Science, Technology, Engineering, Environmental and Ramification Researches 2020*; pp. 222–226, <https://www.scitepress.org/Papers/2018/100778/100778.pdf>.
62. Ju, X.; Bowden, M.; Brown, E.E.; Zhang, X. An Improved X-Ray Diffraction Method for Cellulose Crystallinity Measurement. *Carbohydr. Polym.* **2015**, *123*, 476–481, <https://doi.org/10.1016/j.carbpol.2014.12.071>.
63. Carrillo, I.; Mendonça, R.T.; Ago, M.; Rojas, O.J. Comparative Study of Cellulosic Components Isolated from Different Eucalyptus Species. *Cellulose* **2018**, *25*, 1011–1029, <https://doi.org/10.1007/s10570-018-1653-2>.
64. Maciel, M.M.Á.D.; de Carvalho Benini, K.C.C.; Voorwald, H.J.C.; Cioffi, M.O.H. Obtainment and Characterization of Nanocellulose from an Unwoven Industrial Textile Cotton Waste: Effect of Acid Hydrolysis Conditions. *Int. J. Biol. Macromol.* **2019**, *126*, 496–506, <https://doi.org/10.1016/j.ijbiomac.2018.12.202>.
65. Xu, C.; Zhu, S.; Xing, C.; Li, D.; Zhu, N.; Zhou, H. Isolation and Properties of Cellulose Nanofibrils from Coconut Palm Petioles by Different Mechanical Process. *PLoS One* **2015**, *10*, e0122123, <https://doi.org/10.1371/journal.pone.0122123>.
66. Manfredi, L.B.; Rodríguez, E.S.; Władka-Przybylak, M.; Vázquez, A. Thermal Degradation and Fire Resistance of Unsaturated Polyester, Modified Acrylic Resins and Their Composites with Natural Fibres. *Polym. Degrad. Stab.* **2006**, *91*, 255–261, <https://doi.org/10.1016/j.polyimdegradstab.2005.05.003>.
67. Martins, D.F.; de Souza, A.B.; Henrique, M.A.; Silvério, H.A.; Neto, W.P.F.; Pasquini, D. The Influence of the Cellulose Hydrolysis Process on the Structure of Cellulose Nanocrystals Extracted from Capim Mombaça (*Panicum Maximum*). *Ind. Crops Prod.* **2015**, *65*, 496–505, <https://doi.org/10.1016/j.indcrop.2014.10.035>.

68. Jacobs, C.; Müller, R.H. Production and Characterization of a Budesonide Nanosuspension for Pulmonary Administration. *Pharm. Res.* **2002**, *19*, 189–194, <https://doi.org/10.1023/A:1014276917363>.
69. Mirhosseini, H.; Tan, C.P.; Hamid, N.S.A.; Yusof, S. Effect of Arabic Gum, Xanthan Gum and Orange Oil Contents on ζ -Potential, Conductivity, Stability, Size Index and PH of Orange Beverage Emulsion. *Colloids Surfaces A Physicochem. Eng. Asp.* **2008**, *315*, 47–56, <https://doi.org/10.1016/J.COLSURFA.2007.07.007>.
70. Araya-Chavarría, K.; Rojas, R.; Ramírez-Amador, K.; Sulbarán-Rangel, B.; Rojas, O.; Esquivel-Alfaro, M. Cellulose Nanofibers as Functional Biomaterial from Pineapple Stubbles via TEMPO Oxidation and Mechanical Process. *Waste and Biomass Valorization* **2022**, *13*, 1749–1758, <https://link.springer.com/article/10.1007/s12649-021-01619-3>.
71. Fitriani, F.; Aprilia, S.; Arahman, N.; Bilad, M.R.; Amin, A.; Huda, N.; Roslan, J. Isolation and Characterization of Nanocrystalline Cellulose Isolated from Pineapple Crown Leaf Fiber Agricultural Wastes Using Acid Hydrolysis. *Polymers* **2021**, *13*, 4188. <https://doi.org/10.3390/polym13234188>.
72. Satyamurthy, P.; Jain, P.; Balasubramanya, R.H.; Vigneshwaran, N. Preparation and Characterization of Cellulose Nanowhiskers from Cotton Fibres by Controlled Microbial Hydrolysis. *Carbohydr. Polym.* **2011**, *83*, 122–129, <https://doi.org/10.1016/j.carbpol.2010.07.029>.
73. Angellier, H.; Putaux, J.L.; Molina-Boisseau, S.; Dupeyre, D.; Dufresne, A. Starch Nanocrystal Fillers in an Acrylic Polymer Matrix. *Macromol. Symp.* **2005**, *221*, 95–104, <https://doi.org/10.1002/MASY.200550310>.
74. Boluk, Y.; Danumah, C. Analysis of Cellulose Nanocrystal Rod Lengths by Dynamic Light Scattering and Electron Microscopy. *J. Nanoparticle Res.* **2013**, *16*, 1–7, <https://doi.org/10.1007/S11051-013-2174-4>.
75. Mahfoudhi, N.; Boufi, S. Nanocellulose as a Novel Nanostructured Adsorbent for Environmental Remediation: A Review. *Cellulose* **2017**, *24*, 1171–1197, <https://doi.org/10.1007/S10570-017-1194-0>.
76. Uddin, M.; Islam, M.; Das, S. A Novel Biosorbent, Water-Hyacinth, Uptaking Methylene Blue from Aqueous Solution: Kinetics and Equilibrium Studies. *Int. J. Chem. Eng.* **2014**, *2014*, <https://doi.org/10.1155/2014/819536>.
77. Chan, C.H.; Chia, C.H.; Zakaria, S.; Sajab, M.S.; Chin, S.X. Cellulose Nanofibrils: A Rapid Adsorbent for the Removal of Methylene Blue. *RSC Adv.* **2015**, *5*, 18204–18212, <https://pubs.rsc.org/en/content/articlelanding/2015/ra/c4ra15754k>.
78. Wong, S.; Ghafar, N.A.; Ngadi, N.; Razmi, F.A.; Inuwa, I.M.; Mat, R.; Amin, N.A.S. Effective Removal of Anionic Textile Dyes Using Adsorbent Synthesized from Coffee Waste. *Sci. Rep.* **2020**, *10*, 1–13, <https://doi.org/10.1038/s41598-020-60021-6>.
79. Mutar, H.R.; Jasim, K.K. Adsorption Study of Disperse Yellow Dye on Nanocellulose Surface. *Mater. Today Proc.* **2022**, 1–7, <https://doi.org/10.1016/j.matpr.2021.04.003>.
80. Coir Board Market Rates of Coir and Coir Products in Pollachi; **2021**. http://coirboard.gov.in/?page_id=259.
81. Cellulose Lab Cellulose Lab | Nanocellulose, Cellulose NanoCrystal (CNC or NCC), Cellulose Nanofibrils (CNF) and Bacterial Cellulose (BC) Supplier - Provide the Most Diversified Nanocellulose Products / Cellulose Nanomaterials in the Market: <https://www.celluloselab.com>.
82. Nelson, K.; Retsina, T.; Iakovlev, M.; Heiningen, A. van; Deng, Y.; Shatkin, J.A.; Mulyadi, A. American Process: Production of Low Cost Nanocellulose for Renewable, Advanced Materials Applications. In *Materials research for manufacturing*. Springer **2016**; 267–302, https://link.springer.com/chapter/10.1007/978-3-319-23419-9_9.

Supplementary materials

Table S1. Economics of nanocellulose synthesis.

S.No.	Particulars	Quantity	Unit	Rate (Rs.)	Amount (Rs.)
A. Raw material					
1	Coir Husk	5	kg	13	65.00
2	Sulphuric Acid	25.5	L	165	4207.50
3	Nitric Acid	5	L	174	867.50
4	Sodium Hydroxide	1.25	kg	185	231.25
5	Sodium Hypochlorite	50	L	31	1550.00
B. Processing Cost					
1	Electricity	13.2	unit	8	105.60
C. Others					
1	Water & unsorted materials				2000.00
2	Miscellaneous				138.70
				Total	9166.00